

See discussions, stats, and author profiles for this publication at: <https://www.researchgate.net/publication/341388147>

In-Plane Response of Perforated Unreinforced Masonry Walls under Cyclic Loading: Experimental Study

Article in *Journal of Structural Engineering* · June 2020

DOI: 10.1061/(ASCE)ST.1943-541X.0002657

CITATIONS

0

READS

116

3 authors, including:



Milon Kanti Howlader
University of Newcastle

18 PUBLICATIONS 69 CITATIONS

[SEE PROFILE](#)



M. C. Griffith
University of Adelaide

216 PUBLICATIONS 3,636 CITATIONS

[SEE PROFILE](#)

Some of the authors of this publication are also working on these related projects:



Design Equations for FRP Anchors to Strengthen Existing RC Buildings [View project](#)



Out-of-Plane Assessment of Unreinforced Masonry walls Under Earthquake Loading [View project](#)

In-Plane Response of Perforated Unreinforced Masonry Walls under Cyclic Loading: Experimental Study

M. K. Howlader¹; M. J. Masia² and M. C. Griffith³

Abstract: This paper presents the results of an experimental study into the behavior of perforated (containing openings) unreinforced masonry (URM) walls subjected to cyclic in-plane lateral loading. Damage to perforated URM walls during previous earthquakes has revealed that the in-plane response is mainly influenced by the pier and spandrel geometry, as well as the level of axial compressive stress on the walls due to gravity loading. The study focused on masonry typologies representative of historical URM buildings in the Australian context. To investigate this behavior, eight full-scale URM walls with semicircular arched openings, double wythe thickness, and materials representing masonry construction from the mid 19th to mid 20th century were constructed for pseudo-static cyclic in-plane testing. The experimental program considered varying spandrel depths and pier widths and the imposed vertical loading on the piers was also varied to observe the lateral load capacity and the variation of pier-spandrel failure modes. The test results showed that the in-plane capacity and the failure modes were significantly affected by changes of wall geometry and the imposed vertical pre-compression loading. Predictions of wall strengths, in-plane stiffnesses and failure modes according to American Society of Civil Engineers (ASCE) guidelines show that the guidelines agree well with the test observations.

Keywords: perforated unreinforced masonry, experimental, in-plane response, seismic capacity.

¹PhD Student, Centre for Infrastructure Performance and Reliability, The University of Newcastle, Callaghan NSW 2308, Australia (corresponding author). Email: MilonKanti.Howlader@uon.edu.au

²Associate Professor, Centre for Infrastructure Performance and Reliability, The University of Newcastle, Callaghan, NSW 2308, Australia. Email: mark.masia@newcastle.edu.au

³Professor, School of Civil, Environmental and Mining Engineering, The University of Adelaide, North Terrace Campus, SA 5005 Australia. Email: michael.griffith@adelaide.edu.au

Introduction

Seismic assessment of existing URM buildings is an important concern, as these structures showed poor performance during past earthquake events throughout the world (Melchers 1990; Ingham and Griffith 2011; Griffith et al. 2013). The most common construction practice from the early settlement to the middle of the 20th century in Australia was unreinforced masonry (Howlader et al. 2016). At the time of those URM constructions, there was no earthquake resistance building code in Australia so many such existing buildings are non-compliant with modern design standards. The damage to URM structures in the 1989 Newcastle earthquake of magnitude M5.6 showed the seismic vulnerability of the older URM structures in Australia. A large number of URM structures in Australia have important heritage value and so there is a strong desire to preserve them for future generations. These structures are deteriorating slowly due to the aging of the materials and are vulnerable to severe natural events like earthquakes, which threaten not only the buildings themselves, but also present a threat to the life safety of occupants and passers-by (Tomazevic 1999). Hence, it is necessary to develop reliable models to assess the behaviour and safety of URM buildings under seismic actions considering the location and importance of the structures. Such models can better inform decision makers regarding the timing and extent of structural strengthening measures for existing buildings.

URM buildings are typically composed of several load bearing and partition walls oriented in orthogonal directions with flexible diaphragms at floor and roof levels. For the seismic assessment of the buildings, in-plane (walls aligned parallel to the direction of seismicity) and out-of-plane (walls aligned orthogonal to the direction of seismicity) actions are taken into consideration. Out-of-plane failure of walls can be minimised by proper connection between the walls and diaphragms. However, the global stability of such buildings depends on the behavior of the load

bearing in-plane URM walls, the seismic capacity of which depends on the strength and ductility of the walls. These properties are the resultant of the masonry material properties, the geometry of the wall, building configuration and the loading conditions.

Perforated in-plane loaded URM walls, which contain window and/or door openings, show greater vulnerability due to seismic events, compared to solid walls. The openings in a wall divide the wall into a series of vertical (pier) and horizontal (spandrel) components. Previous research into the behaviour of perforated URM walls was most often dedicated to the pier only to represent and assess the global behaviour of the walls. Therefore, assessment was based on the performance of the piers considering only the weak or strong coupling effect of spandrels on piers. This resulted in assessment guides for existing URM walls such as NZSEE (2006). However based on past earthquake observations, the spandrels also showed extensive damage along with piers (Dizhur et al. 2010). Some researchers (Yi et al. 2006; Nateghi and Alemi 2008; Bothara et al. 2010; Augenti et al. 2011; Kalali and Kabir 2012; Vanin and Foraboschi 2012; Parisi et al. 2014; Triller et al. 2016; Allen et al. 2016; Knox et al. 2016) have conducted testing programs using full or reduced scale perforated walls to better understand the importance of the behaviour of spandrels on the global response of walls. Recently, a few researchers (Foraboschi 2008; Beyer and Dazio 2012; Gattesco 2016) have performed full scale spandrel tests with different types of lintels to study the influence of spandrels in URM walls under in-plane shear forces.

The aim of the testing program reported in this paper is to contribute to the understanding of the lateral in-plane load capacity and the failure modes for perforated URM walls, which represent heritage clay masonry in Australia. The focus was to quantify the influence on the wall behavior of variations of pier and spandrel aspect ratios and the level of vertical axial load to represent variations in gravity loads for walls at different heights within a multi-storey building. The results

from the reported testing program are being used for the calibration of finite element models of wall and building behaviour. The broader aim of the project is to assist researchers and design engineers to develop more reliable models to assess the seismic performance of in-plane loaded URM walls and older existing URM buildings.

Experimental Program

Eight full-scale perforated URM walls of three different geometries were constructed in the structural engineering laboratory at The University of Newcastle, Australia. The walls were designed to represent a single storey section of wall from a larger building façade typical of heritage URM buildings in Australia. A typical heritage building facade in New South Wales (NSW) Australia is shown in Fig. 1.

Seven walls were made with the same overall length and height of the wall but with variations in the pier and spandrel aspect ratios achieved by varying the depth of the spandrel. The eighth wall was constructed with asymmetric pier lengths by increasing the length of one of the piers. All the walls were constructed with the same type of clay brick and same mortar mix design and were tested under quasi-static cyclic in-plane loading using the same boundary conditions. The level of vertical pre-compression imposed on the walls was varied and for three of the combinations of geometry and pre-compression, two theoretically identical specimens were tested.

Geometry of wall specimens

The test specimens were intended to represent the URM walls typically found in the heritage buildings in Australia. A study by Howlader et al. (2016) shows that most heritage listed buildings

in the Australian state of New South Wales (NSW) were constructed before 1930 using clay bricks. The building construction practice at that time was mainly confined to the use of solid walls, of multi-wythe thickness constructed using the so-called common bond pattern (Lucas, 1982). This bond pattern includes wythes consisting of courses of stretcher units which are connected together at regular intervals by courses of header units. The shape of window and door openings in heritage buildings in the NSW region vary between rectangular, semi-circular, segmental and gothic (common in church buildings) but the most common observed shape for openings in Newcastle, Australia is the semicircular arch headed opening. A detailed study for the choice of geometry is described in Howlader et al. (2018).

Considering the abovementioned characterisations, the three test specimen geometries shown in Fig. 2 were chosen. These geometries represent single storey sections within a large perforated wall in the late 19th and early 20th century constructed buildings. The walls consisted of two URM piers laterally connected by a semicircular arched spandrel as shown in Fig. 2. The overall height of each wall is 2398 mm and the lengths are 2630 mm or 2990 mm. With the change of the spandrel depth and the pier lengths, the walls had different pier and spandrel aspect ratios. All of the walls were made with the same masonry bond pattern with a two wythe thickness of 230 mm as shown in Fig. 2 (d). In this arrangement, the header courses were laid at every fourth course to connect tightly the two leaves (wythes) of the wall. Four walls of the shallow spandrel geometry (Fig. 2 (a)), three walls of the deep spandrel geometry (Fig. 2 (b)) and one wall of the asymmetric geometry (Fig. 2 (c)) were constructed.

Selection of materials and properties

Solid dry-pressed new clay brick units of common available dimensions 230 mm (length) x 110 mm (thickness) x 76 mm (height) were used to construct the wall specimens. The bricks used to

construct heritage buildings may have some differences in properties and characteristics compared to more modern bricks, especially regarding the manufacturing process. To represent the behavior of heritage masonry one approach is to use recycled bricks from the demolition of URM buildings constructed at a similar time to the buildings of interest. However, it is not possible to obtain the correct nature of the bond between the brick unit and mortar as a thin layer of original mortar remains adhered to the recycled brick surface. As the unit-mortar bond strength was expected to have a significant impact on the in-plane shear response of the URM walls, recycled bricks were not used in the current study. Instead, new solid dry pressed units with low compressive strength and with typically higher suction properties (rather than the more commonly available extruded units) were used to provide the closest possible replication of heritage clay brick masonry.

The selection of mortar was based on compressive and tensile bond strength tests of several trial mortar combinations to identify a mortar design which could reproduce mortar similar to that used at the time of heritage construction. Before the Napier earthquake in 1931 the URM building construction practice in Australia was similar to that of New-Zealand. Tests on mortar by Lumantarna (2012) for URM heritage buildings in New-Zealand showed a large variation of mortar compressive strengths ranging from 0.53 MPa to 8.58 MPa. Also, volumetric binder to aggregate ratio of 1:3 was found from the acid degradation test (Lumantarna 2012) and by mineralogical separation it was found that the mortar was lime dominated.

Considering the above mentioned research and the knowledge from the local heritage experts in Australia, rock (quick) lime mortar with lime to sand ratio of 1:3 was initially selected for the current study. Masonry prisms (for bond wrench testing) and mortar cubes (for mortar compressive strength testing) were constructed in the laboratory with different types of lime (rock lime and hydrated lime) with or without pozzolan and some with cement. River sand with nominal

maximum size of 4.75 mm was used as aggregate. The gradation curve of the sand is shown in Fig. 3.

For each mortar mix design, the flexural tensile strength of the mortar bed joints was determined using the bond wrench test in accordance with AS3700 (Standards Australia, 2018) at different ages to assess the rate of strength gain. Compressive strength of the mortar was determined by ASTM C109 (ASTM 2016). The results are summarised in Table 1. It can be observed from Table 1 that mortar mixes which contained no cement experienced very slow strength gain. This made them impractical for use in the proposed wall testing program, as the walls had to be built in-situ in the testing location one at a time, cured and tested before the next wall could be built.

Considering the need to represent materials typical of heritage construction, and the need for a mortar with sufficient strength gain for testing of walls at 28 days, a lime rich cement-lime mortar was selected for the proposed testing program. The chosen mortar, which is shown in the second last row in Table 1 has mix proportions by volume of 1 cement : 2 lime (rock) : 9 sand. This mortar falls into the AS3700 'M2' (Standards Australia 2018) or ASTM 'O' (ASTM 2014) classification. This mortar is low in strength and can represent the weather deteriorated mortar of heritage buildings. All mortar joints in the test walls (bed, perpend and collar joints) were 10 mm thick and completely filled with mortar.

After selecting the materials for this testing program, the mechanical properties of the brick, mortar and the masonry were obtained according to the standard test methods, which are shown in Table 2.

The walls were constructed by professional bricklayers under close supervision. For constructing each wall, two mortar batches were used and for each mortar batch 10 mortar joints were prepared to determine the masonry flexural tensile bond strength in accordance with AS3700 (2018). The

bond wrench testing was conducted at the same age as the wall constructed using that mortar was tested. The mortar curing time was at least 28 days prior to wall testing. The first wall tested had a much longer curing time due to delays in commencing the testing program. The direct tensile strength of the mortar joint (f_{jt}) was obtained from the flexural bond strength (f_{mt}) by dividing by a factor of 1.5 as proposed by Van der Pluijm (1997). The values for every batch of mortar used in the wall construction are shown in Table 3. In Table 3, the walls are identified according to spandrel type_pre-compression level_test repetition. For instance, WS_0.2_A represents the shallow spandrel wall geometry with 0.2 MPa pre-compression stress in each pier and A is for the first of two tests for this combination.

In this testing program from the observation of the low variability between repeated tests, the repeat test for the wall type with deep spandrel and low pre-compression level (WD_0.2) was skipped and test WD_0.4/0.7 was introduced. The wall WD_0.4/0.7 represents the wall with asymmetric pier width resulting in 0.4 MPa pre-compression in left pier (longer pier) and 0.7 MPa pre-compression in the right pier (shorter pier).

Test set-up

The experimental setup used for the cyclic in-plane lateral load tests is shown in Fig. 4. The walls were constructed in-situ on a mortar bed on top of a composite steel/reinforced concrete footing beam. The beam consisted of a steel channel (300 PFC) section bolted to the laboratory strong floor, with a reinforced concrete beam cast between the flanges to make the upper surface of the beam concrete.

Vertical pre-compression load representing the gravity load on the wall was applied at the centre of each pier using the vertically aligned hydraulic actuator. The lower (0.2 MPa) and higher (0.5 MPa and 0.7 MPa in the case of WD_0.4/0.7) levels of vertical pre-compression were selected to

represent the average compressive stresses due to gravity loads for walls in the upper and lower stories of a typical three to four storey URM building, respectively. The vertical load was transferred to the centre line of the piers through the spreader beam (250UC 72.9). To help achieve a uniform distribution of the vertical load throughout the pier cross sections, additional steel beam sections of 200UC 46.2 covering the length of each pier were attached above the main loading beam (200UC 46.2).

Lateral displacement was applied at the mid-length of the loading beam (200UC 46.2). The horizontal hydraulic actuator reacted against the laboratory strong wall (Fig. 5) and was connected to the centre point of the loading beam via steel loading arms. Composite steel beam sections (300 PFC with top plate and stiffener) were placed along the pier lengths between the wall and loading beam to allow vertical movement of the spandrel during cyclic lateral movement of the walls. These beams were bolted to the loading beam above and the bottom surface was attached to the top edge of the wall specimens using high strength epoxy. The complete assembly of steelwork at the upper surface of the wall, including the stiffness of the chosen steel sections, was designed by Allen et al. (2014) to represent the restraint experienced by a URM pier-spandrel sub-assembly (frame) within a larger multi-storey wall including another similar masonry frame on the storey above. The boundary condition along the upper edge of the wall allowed in-plane rotation of the pier-spandrel sub-assembly. The gap provided immediately above the spandrel was designed to represent the presence of another opening above the spandrel in a multi-storey building façade.

The first brick course was restrained against sliding along the concrete footing surface using rectangular hollow box steel sections with end steel plates. Therefore, the sliding and/rocking failure were allowed to occur through the mortar joint in between the first and second brick courses.

Instrumentation

Load cells were connected to the vertical and horizontal hydraulic actuators to measure the vertical and horizontal loads applied to the specimens, respectively. Linear variable differential transformers (LVDTs) were attached at several locations on the wall to measure and monitor the displacements during testing (Fig. 5). The lateral displacement at the mid-length of the loading beam (H11 in Fig. 5) was used for lateral displacement control. The force applied by the horizontal actuator (lateral load) plotted against the displacement at H11 represents the lateral load-displacement response reported in the experimental results section. The other LVDTs were used to capture the horizontal, vertical, and diagonal displacements and/or rotations for each individual element (pier, spandrel and joints) of the tested wall. All instrumentation was connected to a data acquisition system and outputs were continuously logged during testing.

In addition to the hard-wired instruments described above, Digital Image Correlation (DIC) technique was also used to investigate the crack patterns and the displacements on one face of the wall continuously during each test. As the DIC speckle pattern was applied on the front side of the specimens as viewed in Fig. 5, then the LVDTs were placed on the back surface of the wall.

Loading history

Quasi-static cyclic testing of the URM walls were conducted in two phases. Initially, the prescribed vertical pre-compression load was applied and then held constant to simulate the gravity loads on the piers. Then displacement controlled pseudo-static cyclic in-plane loading was applied through the horizontal actuator. Lateral displacement was applied at H11 in reversing cycles with increasing amplitude and each cycle of the same amplitude was repeated three times

in the form of sinusoidal waves. This loading arrangement was applied using a computer programmed control system to achieve the exact time-displacement history. Push cycle was denoted as positive (+) and pull direction as negative (-) throughout the whole testing program. The tests were terminated when the post-peak lateral load reduced by 20% of the peak load or excessive drift was deemed to have occurred. In the case of flexure failure of the wall specimens, tests were stopped when the top displacement of the walls reached 48 mm, which is equal to 2% drift of the walls. The cyclic lateral displacement history used in the testing program is presented here in Fig. 6. The displacement amplitudes are presented on the graph, where 0.5(0.01) means 0.5 mm displacement applied at a rate of 0.01 mm/sec. As the displacement amplitude was increased the actuator speed was also increased so as to maintain an approximately constant period for each cycle. This form of quasi-static cyclic loading is based on that recommended by Tomazevic (1999).

Experimental Results

Force-displacement hysteretic behaviour

The force (lateral force applied by the horizontal actuator) versus displacement (applied at H11 in Fig. 5) responses of the tested URM walls are presented in Fig. 7. The displacement was applied up to 48 mm. The walls which reached this maximum displacement showed narrow hysteretic loops typical of flexural failure behavior (rocking of piers) and hence there was no significant post peak load drop with increasing displacement. For specimens WS_0.5_B and WD_0.5_A the early stages of testing also displayed pier rocking with narrow hysteresis loops, but in the later stages of testing shear failure developed in the piers, and the hysteresis loops became wider. The specimen

WS_0.5_B showed asymmetric load-displacement behaviour after shear cracking, as only one pier showed diagonal cracking throughout its height and the other pier remained stable with rocking nature.

The testing of wall WD_0.2 showed no shear crack in the pier but the 20% load drop was reached at 32 mm displacement due to significant diagonal failure of the spandrel, hence the test was stopped at the 36 mm displacement cycle. The hysteresis loops of this specimen are not wide enough to indicate shear failure. In the case of the asymmetric pier geometry of wall WD_0.4/0.7, the hysteretic loop is unsymmetrical in push and pull direction from the beginning to the end of the test. The wider hysteretic loop and the post peak strength reduction of this specimen in the pull direction represents shear failure of the left pier. The force in the push direction still showed increasing nature with increasing displacement due to the rocking nature of the right pier. In all of the tests, the ability of the walls to support the imposed vertical load was maintained for the complete test duration.

The tested walls displayed highly nonlinear behavior, where the hysteretic loop shape and the ultimate displacement depend on the failure mode of the piers and spandrel. In this experimental program for each displacement amplitude, three sinusoidal cycles were repeated. The load resistance capacity was slightly greater in first cycle of each displacement magnitude than in second and third cycle. However, the values in the second and third cycle are almost identical. Due to the small variation of the load resistance among the repeated cycles, it is evident that URM walls are not highly affected by the repeated loading of the same displacement cycle.

The test results for all the URM walls are presented in Table 4. Here, V_{max} is the maximum lateral load resistance capacity of the tested wall, $\delta_{V_{max}}$ is the displacement measured at H11 corresponding to V_{max} and $\theta_{V_{max}}$ is the associated drift level (drift is defined as the displacement

applied at H11 divided by the overall wall height). δ_u and θ_u represent the ultimate displacement and drift respectively, where the maximum lateral load dropped by 20% or the tests were terminated. From the table it is shown that the variation of the maximum lateral load between positive and negative directions varies from 2% to 8% where the walls are symmetric. In the case of the asymmetric wall (WD_0.4/0.7), the variation is more than 10% and the load is greater when the longer pier (left) was in compression. The variation in load capacities between repeat wall tests are 4-9 % in push direction and 1-5% in pull direction. The ultimate drift value for walls displaying flexural behavior of the piers varies between 1.3 and 2% (mostly 2%), whereas the value for shear failure of the pier is <1.5% drift (mostly 1%).

Observed damage and failure modes

The initial behavioral response of all the walls was similar, where in the push (+) cycle rocking occurred in left pier and in the pull (-) cycle rocking occurred in the right pier. Where shear failure did occur, it occurred later in the test. In all of the tested walls, combinations of shear and flexural cracking were observed in the spandrel. The spandrel cracks formed through the mortar head and bed joints. At approximately 1% drift, the full length of the bed joint beneath the top masonry course was damaged. This resulted from the top course of units being epoxy bonded to the relatively rigid (compared to the masonry below) steel beam. Hence, the damage observed beneath this level is considered to represent behavior expected in the walls of a real building.

Test WD_0.4/0.7 was performed with asymmetric pier geometry with high pre-compression load. After the first cycle of the 5 mm displacement amplitude, the vertical hydraulic jack slipped sideways, resulting in sudden loss of vertical load, which damaged the mortar joint below the top brick course. Immediately, the test was stopped and the mortar joint was repaired by grouting. The

joint was raked out and repointed with grout from both sides of the wall to a depth of 40 mm. After repair, the test was performed again, starting with the 5 mm displacement cycle.

The crack patterns at the ultimate displacement level in both push (+) and pull (-) direction are presented for each wall in Fig. 8. Digital image correlation (DIC) technique was used, where the movement of the speckle patterns relative to a reference (0 mm displacement) image were analysed. The contour maps of the maximum principal strain were plotted to visualise the crack patterns of the walls. Extensive cracking was observed in the spandrel zone for all the tested walls. For the shallow spandrel walls, due to the in-plane loading there is spreading horizontal cracks through the pier-spandrel connection region. In the deep spandrel walls, diagonal cracks were formed in the spandrel, which also extended to the connection region. With the increase of the pre-compression load, the spandrel damage was more prominent. At higher displacement amplitudes, the centre of the spandrel moved vertically upward due to the extensive damage of the spandrel.

In the case of low pre-compression load, the pier failure was confined to pier rocking and to some extent it came to toe crushing due to the development of compressive stresses exceeding the masonry compressive strength. At high pre-compression levels both shear (diagonal cracking) and rocking behaviors were observed in the piers. Due to the low tensile strength of the brick, the diagonal cracks propagated not only through the mortar, but also extended through the bricks.

Similar behavioural response of perforated URM walls under cyclic in-plane testing was observed by Ashraf et al. (2012); Kalali and Kabir (2012); Parisi et al. (2014); Allen et al. (2016); Knox et al. (2016) and others throughout the world. Also, the tested URM walls' damage patterns are consistent with observed damage patterns during previous earthquakes in Australia, New-Zealand and elsewhere (Melchers and Page 1990; Ingham and Griffith 2011). In the case of multistorey

buildings the damage was more prominent in the spandrels located in the lower storey than the higher stories of the same building (for instance the failure of Avonmore House and T & G Building due to earthquake in New-Zealand). Similar behaviour was found in the testing, where the spandrel failure was more prominent in the case of higher pre-compression levels.

Bilinear idealisation of force displacement response

Envelope curves were fitted to the experimental load-displacement hysteresis loops for each tested wall as displayed in Fig. 7. The envelope curve for each wall was constructed by connecting the peak load points of the first cycle for each displacement amplitude in both positive and negative directions. The envelope curves were then idealised to bilinear curves (ideal elastic-plastic response) assuming equal energy dissipation under the envelope and idealised bilinear force-displacement curve in each case.

Two well recognised bilinearisation procedures were used in this study; being the approaches recommended by Magenes et al. (2008) and ASTM (2011), in order to compare the seismic performance parameters derived using each approach. In both approaches, the equal energy dissipation principle is used, but differences exist in the way the elastic stiffness (k_{el}) is determined. In the Magenes et al. (2008) bilinearisation procedure k_{el} is measured by the ratio of lateral load at $0.70V_{max}$ (first crack load) and its corresponding displacement. Conversely, the first crack load is taken with force equal to $0.40V_{max}$ in accordance with ASTM (2011).

The ultimate displacement (δ_u) is taken as the displacement at which the post peak load drops by 20% of the maximum load (V_{max}) for both approaches. However, in most tests in the current study, the load drop did not exceed 20% of maximum load (V_{max}), hence the last data point of the envelope curve was considered as the ultimate point. In these cases the ultimate displacement

recorded represents a lower bound on the displacement capacity for the wall. After obtaining the values of k_{el} and δ_u , the ultimate shear force (V_u) of the idealised system is determined by the equal energy principle. The graphical representation of the bilinear curves using both procedures along with the envelope curves are shown in Fig. 9 for each wall. Using the bilinearised curves, the ultimate force (V_u), yield displacement (δ_e), elastic stiffness (k_{el}), displacement ductility (μ), over-strength factor (Ω), ductility-related strength reduction factor (q) and the force reduction factor (R) were obtained according to each approach and are presented in Table 5 (Magenes et al. 2008) and Table 6 (ASTM 2011). The parameters are determined using the following equations

$$V_u = \left(\delta_u - \sqrt{\delta_u^2 - \frac{2A_{env}}{K_{el}}} \right) K_{el} \quad (1)$$

$$\delta_e = \frac{V_u}{K_{el}} \quad (2)$$

$$\mu = \frac{\delta_u}{\delta_e} \quad (3)$$

$$\Omega = \frac{V_u}{V_{cr}} \quad (4)$$

$$q = \sqrt{(2\mu - 1)} \quad (5)$$

Where, A_{env} is the area under the envelop curve from zero to the ultimate displacement point (δ_u) and V_{cr} is the first crack load. Other parameters are stated above.

Comparing the plots in Fig. 9 and the calculated parameters in Tables 5 and 6 it is clear that several important parameters commonly used to model the behaviour of URM buildings under earthquake loading are highly sensitive to the assumptions made in establishing a bilinear idealisation of the actual non-linear wall response. Of the two approaches assessed here, the approach proposed by Magenes et al. (2008) returns a significantly lower elastic stiffness and in doing so results in much smaller values for displacement ductility, over-strength factor and force

reduction factor compared to the ASTM (2011) approach. This observation tends to indicate that international standardisation in the approach used for bilinearisation of test data may be of benefit for selecting design parameters for inclusion in codes of practice for earthquake design.

Stiffness Degradation

The formation and propagation of cracking during cyclic loading of the URM walls resulted in the degradation of stiffness with increasing displacement amplitude. To observe the trend of stiffness degradation, the stiffness ($K_{eff,i}$) for the first cycle of each displacement amplitude was compared to the initial stiffness (K_{ini}) and plotted against drift (θ) in Fig.10. The vertical ordinate represents the normalised stiffness (ratio of stiffness at a particular cycle to the initial stiffness). The effective stiffness for the hysteresis cycle ($K_{eff,i}$) was determined according to ASCE 41 (2013) considering both positive and negative quadrants by using the following equation.

$$K_{eff,i} = \frac{|V_i^+| + |V_i^-|}{|\delta_i^+| + |\delta_i^-|} \quad (6)$$

Where, V_i^+ is the peak shear force at a particular cycle i with the corresponding displacement δ_i^+ in the positive quadrant, and V_i^- and δ_i^- represent the peak shear force and corresponding displacement in the negative quadrant of the same cycle, respectively.

The stiffness of only the first cycle of each applied displacement was considered here, as there was no noticeable stiffness degradation among the first, second and third cycles. Fig. 10 shows that the degradation of stiffness is consistent for all specimens. At lower drift levels, the stiffness degradation is reasonably rapid and after the drift level of 0.8%, the degradation rate is almost linear with much lower slope. The effective stiffness degraded to approximately half of the initial

stiffness at a drift level 0.15% and at 0.5% drift level the stiffness was approximately $0.2K_{ini}$. Finally, the best fit curve to correlate the stiffness with the drift level of the tested URM walls is shown by the solid line in Fig. 10 and can be described by the following equation.

$$\frac{K_{eff}}{K_{ini}} = 0.12[\theta + 0.13]^{-1.12} \quad (7)$$

Where, K_{eff} is the effective stiffness at any displacement, K_{ini} is the initial stiffness and θ is the value of drift in %.

Energy dissipation

The energy dissipation achieved during the cyclic URM testing depended on the nature of hysteretic loop and hence on the failure modes observed. It is sometimes difficult to predict the relationship of the dissipated energy with the behavior of the walls as narrow loop hysteresis with high load resistance can dissipate more energy than the wider loop hysteresis with low load resistance. To allow comparison, equivalent viscous damping ratio (ζ_{eq}) was calculated for each wall tested. Equivalent viscous damping ratio is defined as the ratio of the dissipated energy in an actual structure to the energy dissipation capacity of the equivalent viscous system (Chopra 2012). Fig.11 shows the value of ζ_{eq} for each of the three repeated cycles versus drift for the each of the walls. For all of the walls the value of ζ_{eq} shows some irregularities (particularly higher values) at early stages of testing due to the small displacement rate and high stiffness resulting in inconsistent loop formations. For walls which displayed flexural failure modes (pier rocking), the value then stabilizes and remains almost constant with increasing drift, with values for ζ_{eq} lying in

the 5 to 7% range. For the walls which experienced shear failure modes, ζ_{eq} initially remains approximately constant with increasing drift as the flexural behavior dominated, but when the shear failure started to occur, the value of ζ_{eq} increased sharply. In the case of the asymmetric pier geometry, it is unclear why the sharply increasing nature of the damping commenced from approximately 0.33% drift even though the shear failure started at 0.66% drift.

It is also interesting to note that the energy dissipation capacity is decreasing in the repeated cycles of each displacement amplitude. Excluding the unexpectedly higher values of equivalent viscous damping at very small drifts (especially for higher pre-compression levels), the average numerical values are presented in Table 7 to correlate with the wall behavior. The average values consist of the average of all the damping values from the three repeated cycles. From Table 7, it can be seen that the average value of ζ_{eq} is reasonably consistent across all the walls and could be represented by a single value regardless of whether the final failure is flexural or shear. Although the increase in damping in the later stages of testing for those walls displaying shear failure does result in higher average damping for these specimens, the effect is small implying that the final failure mode has little impact on the average value of damping through the whole range of behavior. For asymmetric pier length wall (WD_0.4/0.7), the COV value is higher than the symmetric pier geometries.

Comparison of Experimental Results with American Society of Civil Engineers Guidelines (ASCE 41 (2013))

The measured in-plane response of the URM walls are compared to the ASCE standard (ASCE 41 (2013)). In ASCE 41 (2013) a range of equations are provided, each representing a different potential mode of failure under in-plane lateral loading. Strength prediction requires evaluation of

the various formulae, from which the strength, and the governing failure mode, are based on the lowest calculated capacity. In this context, the potential failure modes under lateral in-plane loading include: pier rocking (V_r), toe crushing (V_{tc}), bed joint sliding (V_{sl}) and diagonal cracking (V_{dt}) which can be expressed as follows:

$$V_r = 0.9(\alpha P_D + 0.5P_w) \frac{L}{h_{eff}} \quad (8)$$

$$V_{tc} = (\alpha P_D + 0.5P_w) \left(\frac{L}{h_{eff}} \right) \left(1 - \frac{f_a}{0.7f_m} \right) \quad (9)$$

$$V_{sl} = v_{me} A_n \quad (10)$$

$$\text{Where, } v_{me} = \frac{0.75 \left(0.75v_{te} + \frac{P_D}{A_n} \right)}{1.5} \quad (11)$$

$$V_{dt} = f_{dt} A_n \beta \sqrt{1 + \frac{f_a}{f_{dt}}} \quad (12)$$

$$\text{Where, } f_{dt} = 0.5c + f_a \mu_f \quad (13)$$

Where, α is the factor for the boundary condition of the wall/pier (1.0 for fixed-fixed and 0.5 for fixed-free condition), P_D is the axial force on the wall cross-section, P_w is the self-weight of the wall, L is the length of the pier, h_{eff} is the effective height of the pier, f_a is the axial compressive stress at the base of the wall/pier due to gravity load, f_m is the masonry compressive strength, v_{me} is the expected bed-joint sliding shear strength, v_{te} is the average bed joint shear strength, f_{dt} is the diagonal tensile strength of the masonry, A_n is the net mortared area of the pier, β is the correction factor for nonlinear stress distribution and depends on the value of (h_{eff} / L) , c is the cohesion, and μ_f is the coefficient of friction, which is equal to $\tan\phi$.

The lateral in-plane stiffness k_{el} was estimated using the following equation (ASCE 41 (2013)):

$$k_{el} = \frac{I}{\left[\frac{h_{eff}^3}{12E_m I_g} + \frac{h_{eff}}{A_v G_m} \right]} \quad (14)$$

Where, E_m and G_m are the masonry elastic and shear moduli respectively, I_g is the moment of inertia for the gross section representing uncracked behaviour, and A_v is the shear area. Other parameters are as stated above. The above Eq. (12) for in-plane stiffness assumes fixed-fixed boundary conditions for wall piers connected by a spandrel.

The experimentally measured maximum lateral load carrying capacities, governing failure modes and the stiffnesses of the tested walls are compared to the estimated responses by ASCE 41 (2013) in Table 8.

From the Table 8 it is shown that the experimentally recorded peak wall strengths fall between the ASCE 41 (2013) predictions for fixed-free and fixed-fixed boundary conditions for all cases except WS_0.2, which lies above both values but very close to the fixed-fixed assumption. The ASCE 41 (2013) equations assuming fixed-fixed boundary conditions predict well the observed strengths in the case of low pre-compression level. However, in case of high pre-compression the ASCE 41 (2013) equations assuming fixed-free boundary conditions provide a closer match to the experimental results.

For wall piers connected by a spandrel, ASCE 41 (2013) recommends the use of the fixed-fixed boundary condition in strength predictions. From the observed crack patterns, spandrel damage is only moderate at lower levels of pre-compression and so the fixed-fixed assumptions results in a close match to the experimental strengths. However, in the case of high pre-compression, the spandrel suffered greater damage resulting in a loss of coupling of the piers so that the boundary

condition at the top of each pier was something between fixed-fixed and fixed-free. This is supported by the observation that the measured wall strengths fall midrange between the fixed-fixed and fixed-free predictions.

As shown in Table 8, ASCE 41 (2013) predicts flexural (rocking and toe crushing) failure in all cases. Both flexure and diagonal shear failures were observed in the tested walls. However, it should be noted that for the same geometry and loading configuration, the test results showed different failure modes between repeat specimens and between piers in the same specimen. Therefore, the ASCE 41 (2013) predictions were generally in good agreement with test observations.

The lateral in-plane stiffnesses predicted using ASCE 41 (2013) are also compared to the elastic stiffnesses obtained from the bilinear curves according to Magenes et al. (2008) and ASTM (2011) for each specimen (Table 8). For the shallow spandrel walls the predicted stiffnesses are closer to Magenes et al. (2008) and for deep spandrel walls are mid-range between the Magenes et al. (2008) and ASTM (2011) values. It is considered that the stiffness predictions agree well with the experimentally observed values, considering the significant variability in stiffnesses between the tested walls and even between loading directions for the same walls (Table 5 and Table 6).

Conclusions

An experimental study was conducted on the force-displacement behavior, failure modes, stiffness degradation and energy dissipation capacities of eight URM walls with semi-circular arched openings representative of heritage masonry construction in Australia. To investigate the in-plane seismic performance of the walls, quasi-static cyclic horizontal loading combined with constant

vertical loading was applied to the specimens. From the comparative test results and observations the following summaries are drawn:

- At low pre-compression levels, representing walls in the upper stories of a URM building, the damage was more confined to the spandrel region with stable pier rocking occurring with increasing drift. In the case of higher pre-compression level, in most cases the piers initially showed a rocking nature and after that shear failure occurred in one or both piers.
- For deep spandrel walls, the diagonal shear failure throughout the spandrels are most prominent whereas for shallow spandrel walls, the failure is mostly shear sliding.
- Rocking mechanism of the piers permits large lateral displacement with no significant decrease of the lateral load capacity. Shear failure of the pier resulted in significant post peak drop of the lateral load capacity. For some walls in the testing program, one pier was damaged by diagonal shear cracking and the other remained stable with rocking nature, hence the hysteretic nature is different in push and pull directions after the formation of the shear failure.
- The asymmetric pier geometry wall showed different hysteretic nature in push and pull directions, where the load capacity was greater when the longer pier was more heavily compressed (pull direction in the test). The longer pier displayed shear failure which was expected as this pier had a lower aspect ratio than the shorter pier.
- The energy dissipation capacity is minimal in the case of pure rocking nature of the piers and it increased with the formation of the shear crack. While shear failure of the piers increases the equivalent viscous damping, a value of approximately 5% provides a good representation across all drift levels regardless of final failure mode.

- The stiffness degradation patterns for all the tested walls followed a similar pattern and can be represented by a power function.
- In most of the tested walls the pier rocking mechanism allowed greater displacement capacity than observed for walls displaying shear failures. However, for WD_0.2, although shear failure was not observed in the piers, the significant diagonal failure of the spandrel resulted in a marked post peak reduction in the resisting force and increase of energy dissipation capacity of the wall.
- The parameters commonly used to model the behavior of URM buildings under earthquake loading are highly sensitive to the assumptions made in establishing a bilinear idealisation of the actual non-linear wall response. Of the two approaches assessed in this study, the approach by Magenes et al. (2008) returns a significantly lower elastic stiffness and in doing so results in much smaller values for displacement ductility, over-strength factor and force reduction factor compared to the ASTM (2011) approach.
- A comparison of test results against predictions of wall strengths, in-plane stiffnesses and failure modes according to ASCE 41 (2013) show that the ASCE guidelines agree well with the test observations. Furthermore, the observed test results compare well with observations of building damage reported following earthquakes in regions with building typologies similar to those tested.

Data Availability Statement

All data, models, or code generated or used during the study are available from the corresponding author by request.

Acknowledgement

The authors gratefully acknowledge the financial support provided by the Australian Research Council via Discovery Project DP160102070. The authors would like to thank to the laboratory staff and postgraduate students at The University of Newcastle for their help at all stages of testing.

References

- Allen, C., Masia, M. J., and Page, A. W. (2014). "Cyclic in-plane shear behaviour of unreinforced masonry walls with openings: Design of experimental testing programme." *Proc., 9th International Masonry Conference*, Guimarães, Portugal.
- Allen, C., Masia, M. J., and Page, A. W. (2016). "Experimental testing of unreinforced masonry walls with openings subjected to cyclic in-plane shear." *Proc., 16th Int. Brick & Block Masonry Conference (IBMAC)*, Padova, Italy.
- ASCE (2013). "Seismic evaluation and retrofit of existing buildings." *ASCE 41-13*, Reston, Virginia, USA.
- Ashraf, M., Khan, A. N., Naseer, A., Ali, Q., and Alam, B. (2012). Seismic behavior of unreinforced and confined brick masonry walls before and after ferrocement overlay retrofitting. *International Journal of Architectural Heritage*, 6(6), 665-688.
- ASTM (2011). "Standard test methods for cyclic (reversed) load test for shear resistance of vertical elements of the lateral force resisting systems for buildings." *E2126-11*, West Conshohocken, PA.
- ASTM (2014). "Standard specification for mortar for unit masonry." *ASTM C270 -14*, West Conshohocken, PA.

- ASTM (2016). "Standard test method for compressive strength of hydraulic cement mortars (using 2-in or 50-mm cube specimens)." *ASTM C109/C 109M-16*, West Conshohocken, PA.
- Augenti, N., Parisi, F., Prota, A., and Manfredi, G. (2011). "In-plane lateral response of a full-scale masonry subassemblage with and without an inorganic matrix-grid strengthening system." *Journal of Composites for Construction*, 15(4), 578-590.
- Beyer, K., and Dazio, A. (2012). "Quasi-static cyclic tests on masonry spandrels." *Earthquake Spectra*, 28(3), 907-929.
- Bothara, J. K., Dhakal, R. P., and Mander, J. B. (2010). "Seismic performance of an unreinforced masonry building: an experimental investigation." *Earthquake Engineering & Structural Dynamics*, 39(1), 45-68.
- Chopra, A. K. (2012). *Dynamics of structures-Theory and applications to earthquake engineering* (Fourth ed.), Pearson-Prentice Hall, Upper Saddle River, NJ.
- Dizhur, D., Ismail, N., Knox, C. L., Lumantarna, R., and Ingham, J. M. (2010). "Performance of unreinforced and retrofitted masonry buildings during the 2010 Darfield earthquake." *Bull. of the New Zealand Society for Earthquake Engineering*, 43(4), 321-339.
- European Standard (2002). "Methods of test for masonry, Part 3: Determination of initial shear strength." *EN1052-3*, European committee of standardization, Brussels, Belgium.
- Foraboschi, P. (2009). "Coupling effect between masonry spandrels and piers." *Materials and Structures*, 42(3), 279-300.
- Gattesco, N., Macorini, L., and Dudine, A. (2015). "Experimental response of brick-masonry spandrels under in-plane cyclic loading." *Journal of Structural Engineering*, 10.1061/(ASCE)ST.1943-541X.0001418, 04015146.

- Griffith, M. C., Moon, L., Ingham, J. M., and Derakhshan, H. (2013). "Implications of the Canterbury earthquake sequence for Adelaide, South Australia." *Proc. 12th Canadian Masonry Symposium*, Vancouver, British Columbia, Canada.
- Howlader, M. K., Masia, M. J., Griffith, M. C., Ingham, J. M., and Jordan, J. W. (2016). "Characterisation of heritage masonry construction in NSW - State Heritage Register." *Proc., Australian Earthquake Engineering Society conference*, Melbourne, Australia.
- Howlader, M. K., Masia, M. J., Griffith, M. C., Ingham, J. M., and Jordan, J. W. (2018). "Design of in-plane unreinforced masonry wall testing program and preliminary finite element analysis (FEA)." *Proc. 10th Australian Masonry Conference*, Sydney, Australia.
- Ingham, J. M., and Griffith, M. C. (2011). "Performance of unreinforced masonry buildings during the 2010 Darfield (Christchurch, NZ) earthquake." *Australian Journal of Structural Engineering*, 11(3), 207-224.
- Kalali, A., and Kabir, M. (2012). "Cyclic behavior of perforated masonry walls strengthened with glass fiber reinforced polymers." *Scientia Iranica*, 19(2), 151-165.
- Knox, C. L., Dizhur, D., and Ingham, J. M. (2016). "Experimental Cyclic Testing of URM Pier-Spandrel Substructures." *Journal of Structural Engineering*, 10.1061/(ASCE)ST.1943-541X.0001650, 04016177.
- Lucas, C. (1982). *Conservation and restoration of buildings-preservation of masonry walls*, Australian Council of National Trust, Australia.
- Lumantarna, R. (2012). "Material characterisation of New Zealand's clay brick unreinforced masonry buildings." PhD Thesis, Department of Civil and Environmental Engineering, The University of Auckland, New Zealand.

- Magenes, G., Morandi, P., and Penna, A. (2008). "Test results on the behavior of masonry under static cyclic in-plane lateral loads." ESECMaSE project, Department of Structural Mechanics, University of Pavia, Italy.
- Melchers, R. E. (1990). *Newcastle earthquake study*, The Institution of Engineers, Australia.
- Melchers, R. E., and Page, A. W. (1990). *Preliminary report on Newcastle earthquake*, The University of Newcastle, NSW 2308, Australia.
- Nateghi, F. A., and Alemi, F. (2008). "Experimental study of seismic behaviour of typical Iranian URM brick walls." *Proc. 14th World Conference on Earthquake Engineering*, Beijing, China.
- NZSEE (2006). "Assessment and improvement of the structural performance of buildings in earthquake -prioritisation, initial evaluation, detailed Assessment, improvement measures, recommendations of a NZSEE study group on earthquake risk buildings." Wellington, New Zealand.
- Parisi, F., Augenti, N., and Prota, A. (2014). "Implications of the spandrel type on the lateral behavior of unreinforced masonry walls." *Earthquake Engineering & Structural Dynamics*, 43(12), 1867-1887.
- Standards Australia (2003a). "Masonry units, segmental pavers and flags—Methods of test, Method 4: Determining compressive strength of masonry units." *AS/NZS 4456.4*, Standards Australia Limited and Standards New Zealand, Australia and New Zealand.
- Standards Australia (2003b). "Masonry units, segmental pavers and flags—Methods of test, Method 15: Determining lateral modulus of rupture." *AS/NZS 4456.15*, Standards Australia Limited and Standards New Zealand, Australia and New Zealand.
- Standards Australia (2018). "Masonry structures." *AS3700*, Standards Australia Limited, Australia.

- Tomažević, M. (1999). *Earthquake resistant design of masonry buildings (Vol. 1)*, Imperial College Press, London.1-86094-066-8.
- Triller, P., Tomažević, M., and Gams, M. (2016). “Seismic behaviour of multistorey plain masonry shear walls with openings: An experimental study.” *Proc., 16th International Brick and Block Masonry Conference*, Padova, Italy.
- Van der Pluijm, R. (1997). Non-linear behaviour of masonry under tension. *HERON*, 42(1), 25-54.
- Vanin, A., and Foraboschi, P. (2012). “In-plane behavior of perforated brick masonry walls.” *Materials and structures*, 45(7), 1019-1034.
- Yi, T., Moon, F. L., Leon, R. T., and Kahn, L. F. (2006). “Lateral load tests on a two-story unreinforced masonry building.” *Journal of Structural Engineering*, 10.1061/ ASCE0733-94452006132:5643, 643-652.

List of Figures



Fig. 1. Frederick Ash Building, Newcastle, NSW, Australia

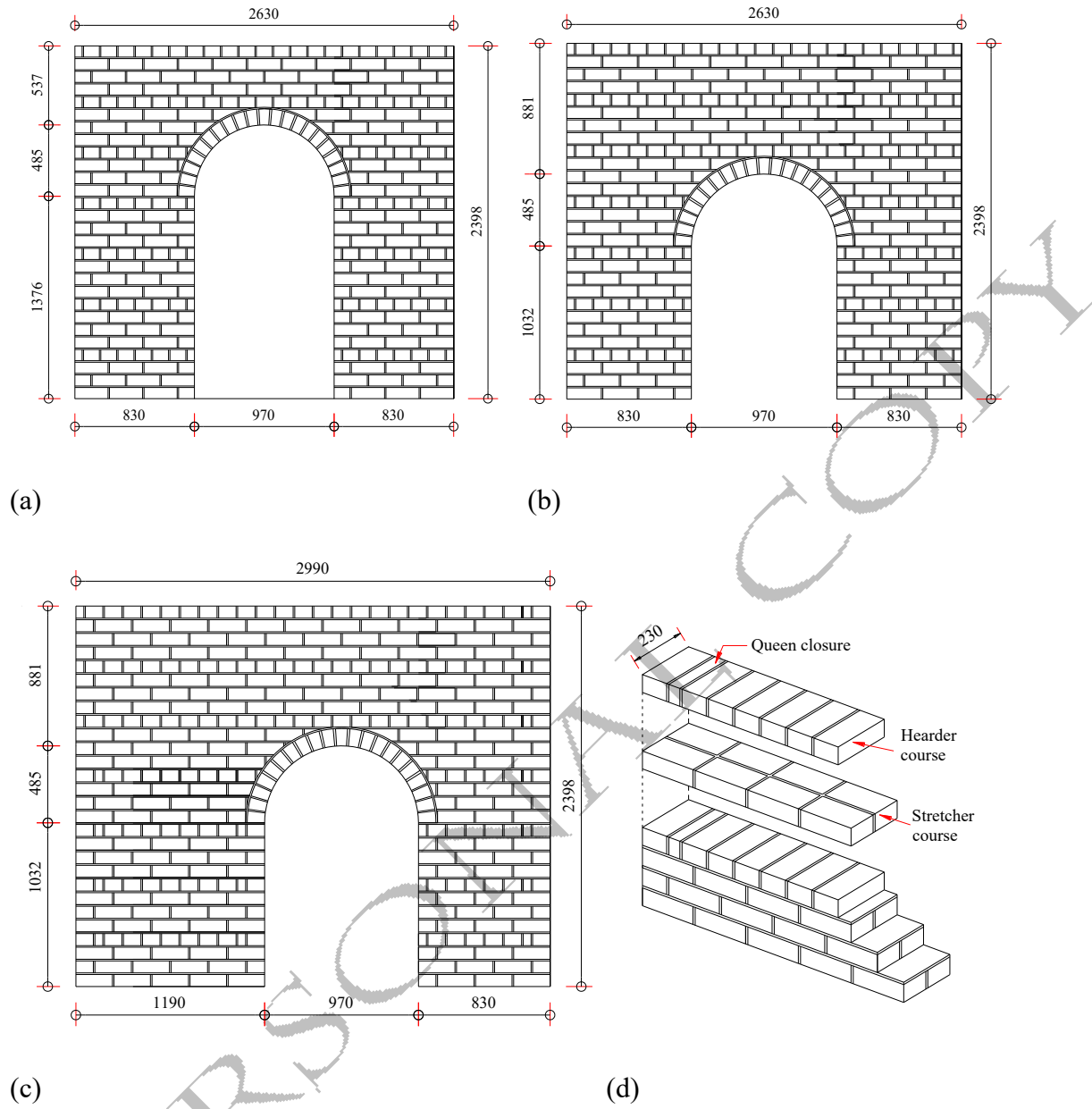


Fig. 2. Wall geometry (all dimensions in mm): (a) shallow spandrel wall (b) deep spandrel wall (c) asymmetric pier wall (d) masonry bond pattern

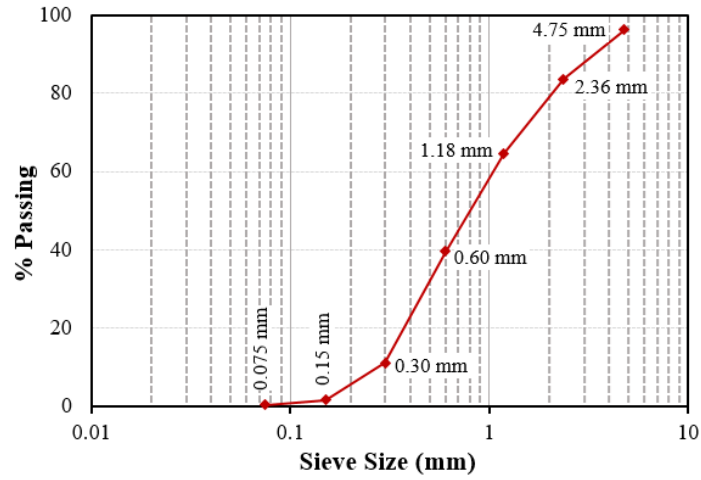


Fig. 3. Sieve analysis of river sand used in the mortar

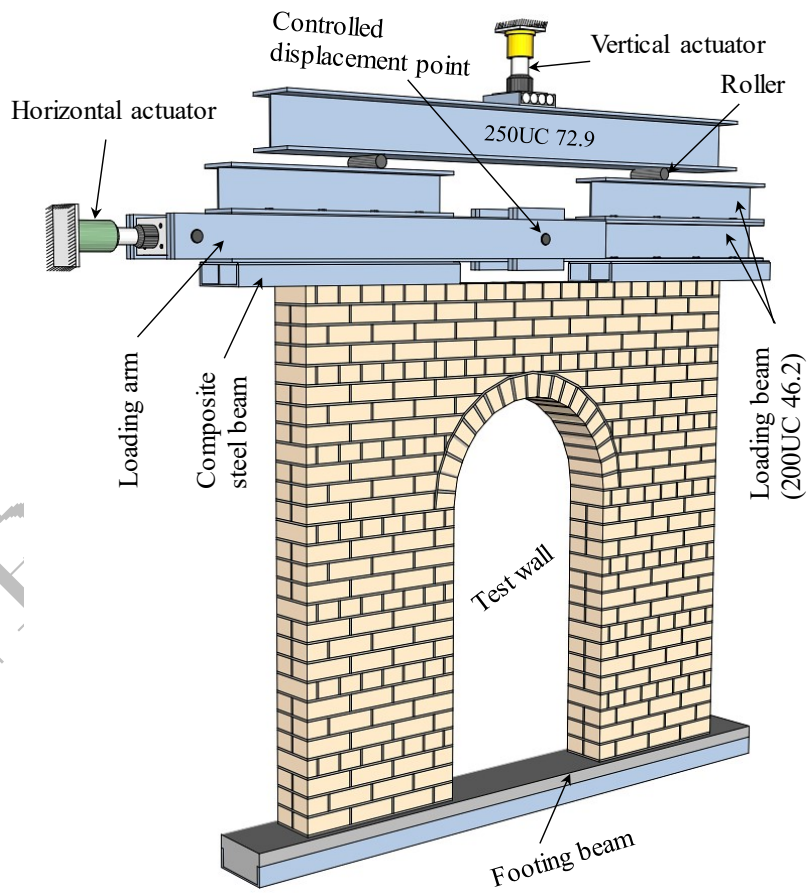


Fig. 4. Diagram of experimental test set-up

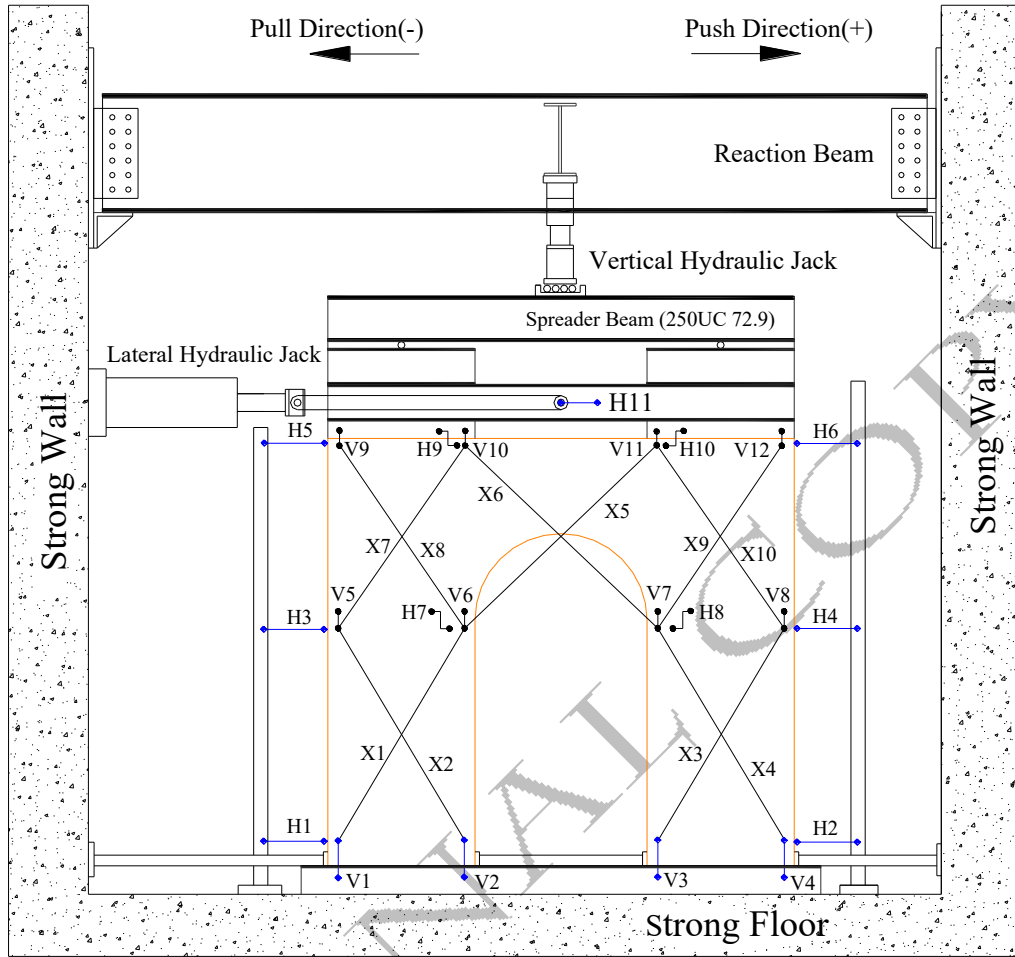


Fig. 5. Instrumentations used in the tested walls (side elevation).

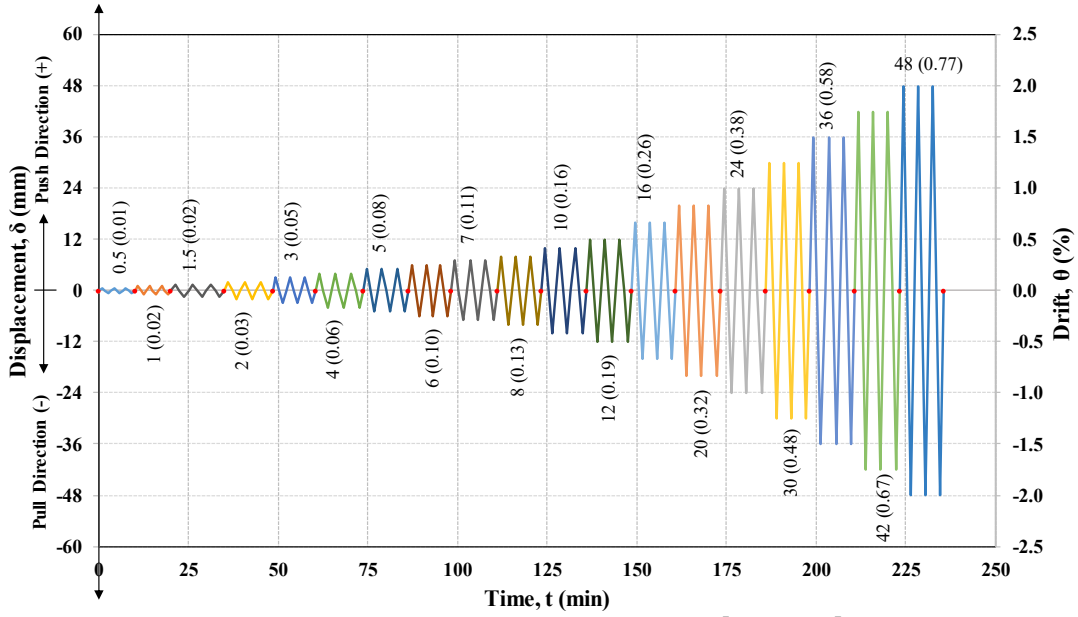
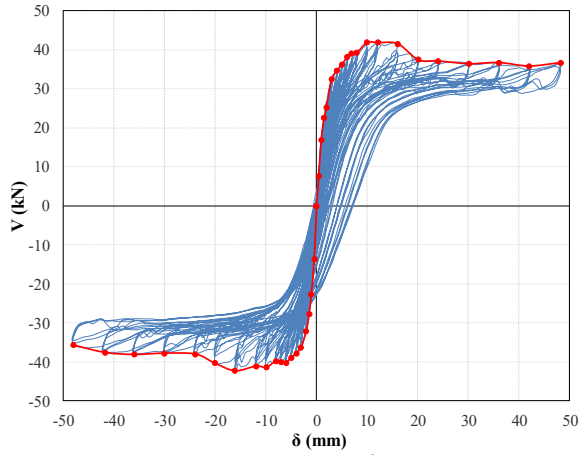
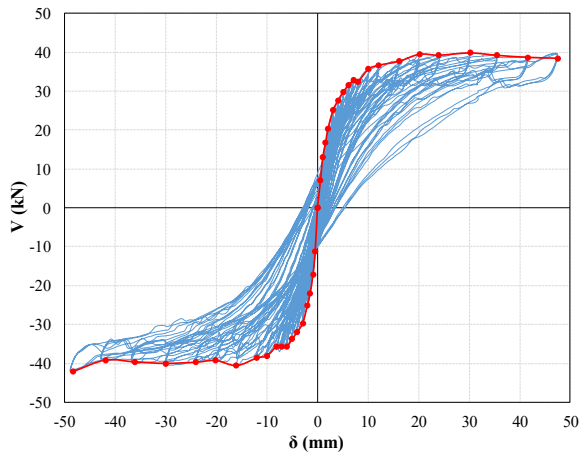


Fig. 6. Applied displacement time history for test specimens

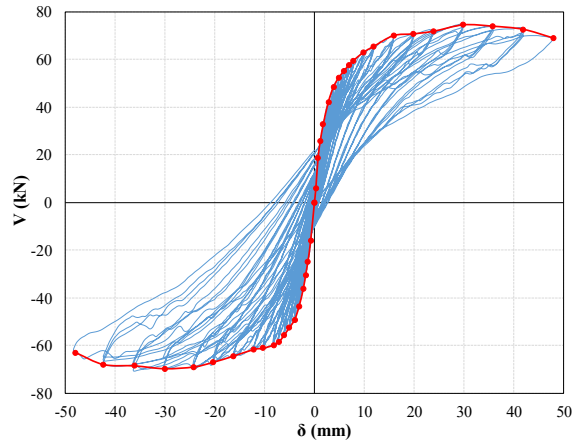


(a) WS_0.2_A

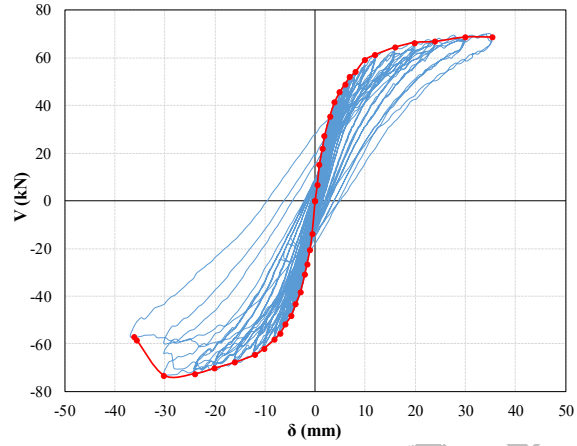


(b) WS_0.2_B

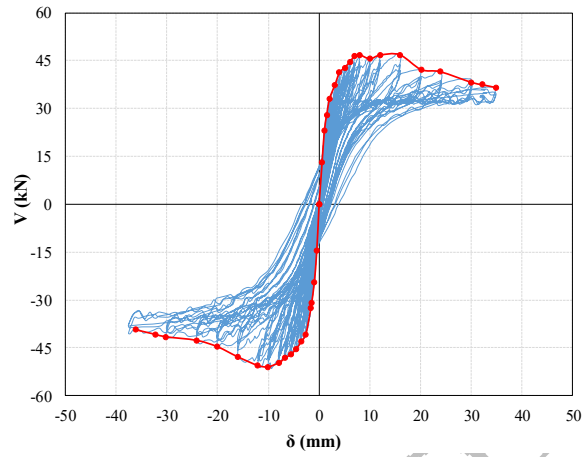
PERK



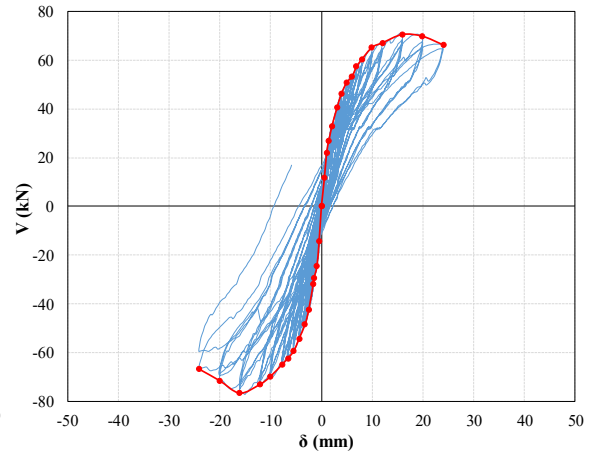
(c) WS_0.5_A



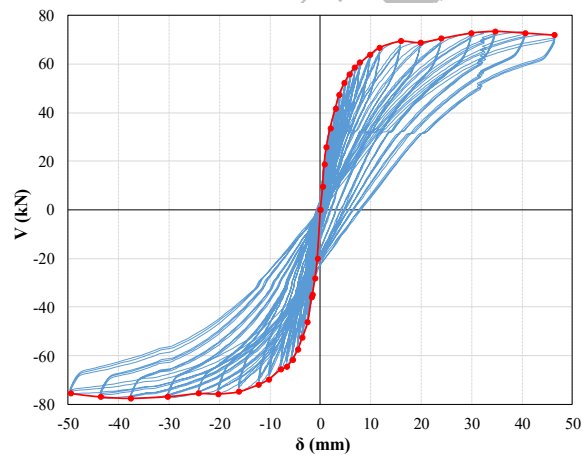
(d) WS_0.5_B



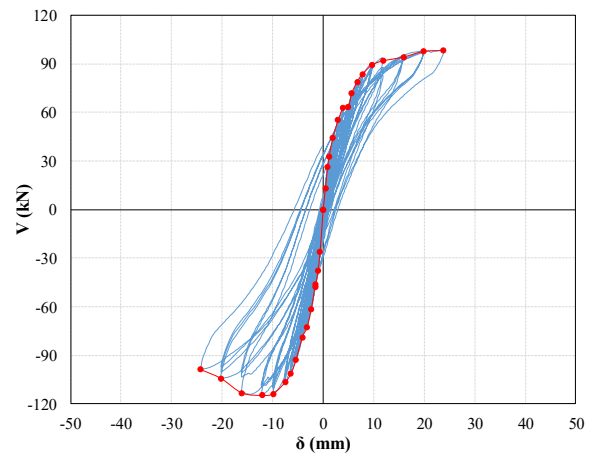
(e) WD_0.2



(f) WD_0.5_A

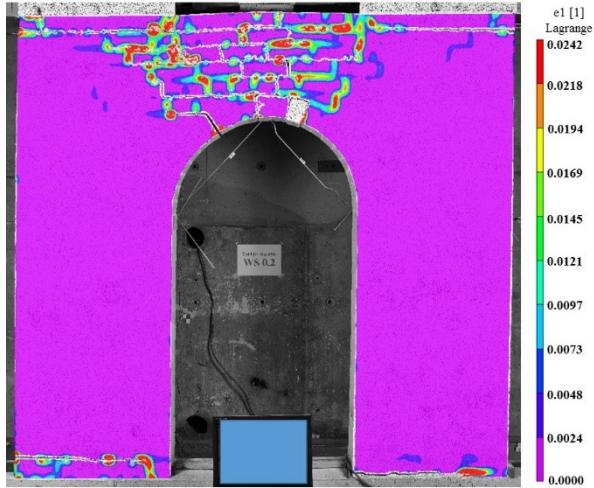


(g) WD_0.5_B

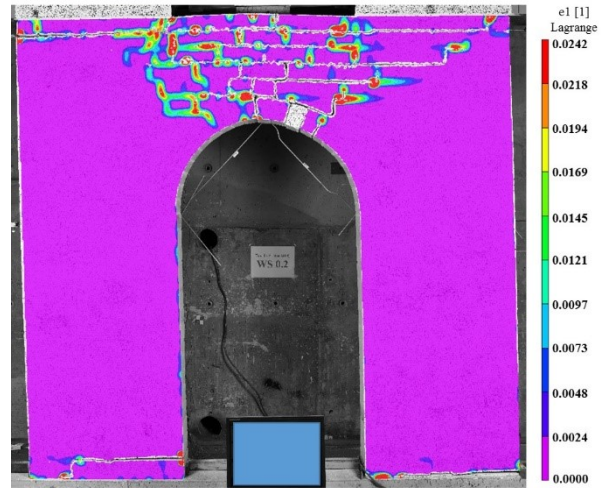


(h) WD_0.4/0.7

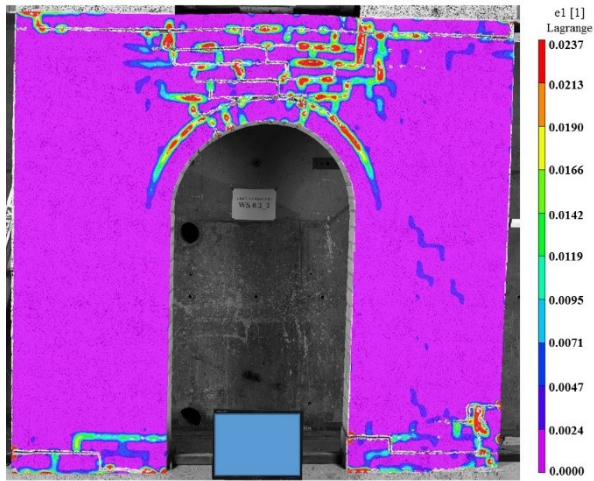
Fig. 7. Force-displacement hysteresis with envelope curve for the in-plane tested walls.



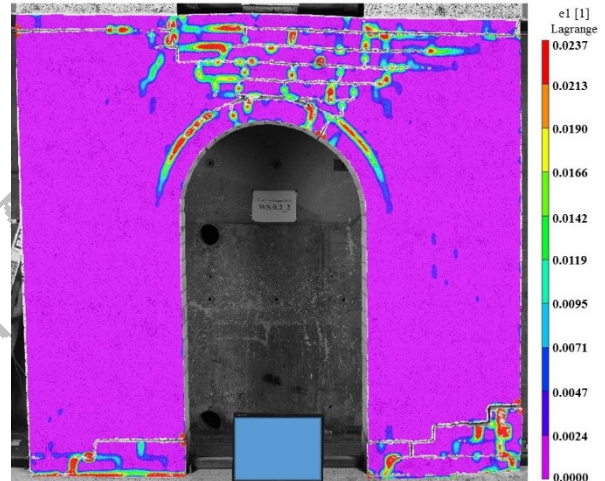
(a) WS_0.2_A (+48.0 mm)



(b) WS_0.2_A (-48.0 mm)

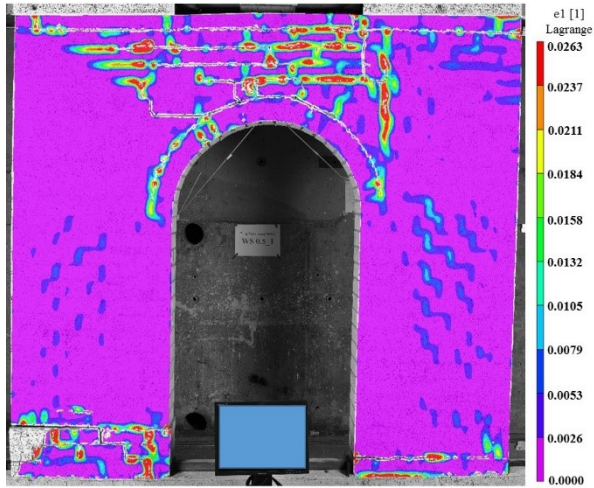


(c) WS_0.2_B (+48.0 mm)

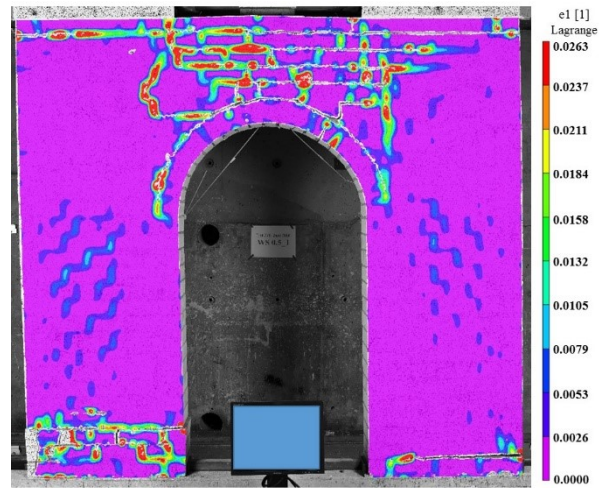


(d) WS_0.2_B (-48.0 mm)

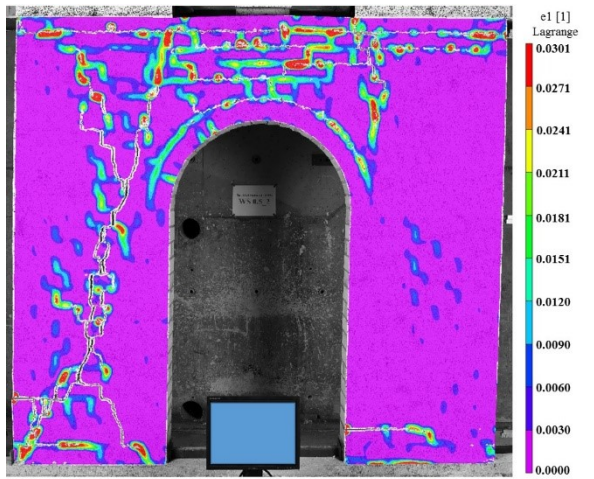
PER



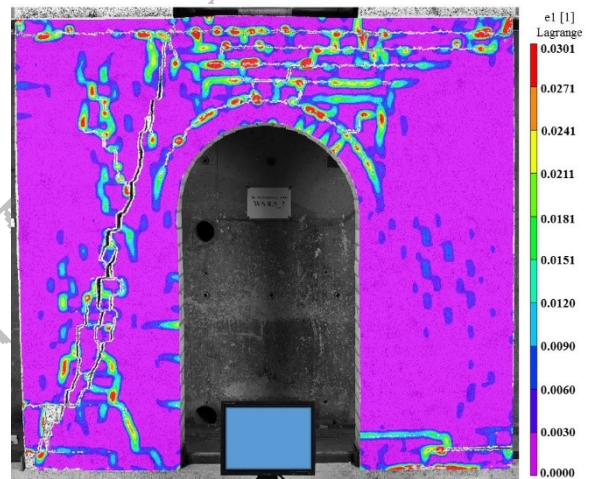
(e) WS_0.5_A (+48.0 mm)



(f) WS_0.5_A (-48.0 mm)

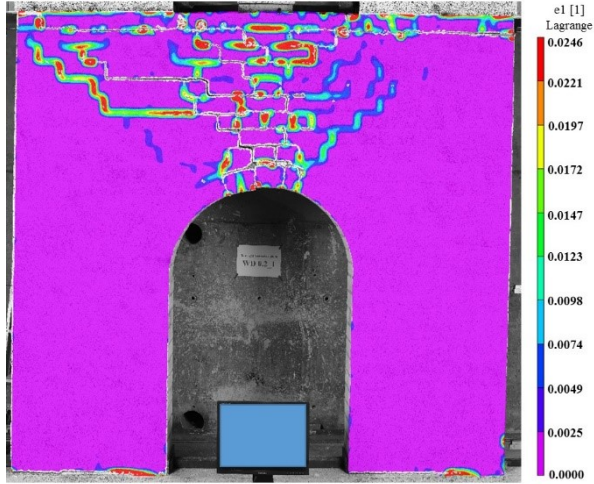


(g) WS_0.5_B (+36.0 mm)

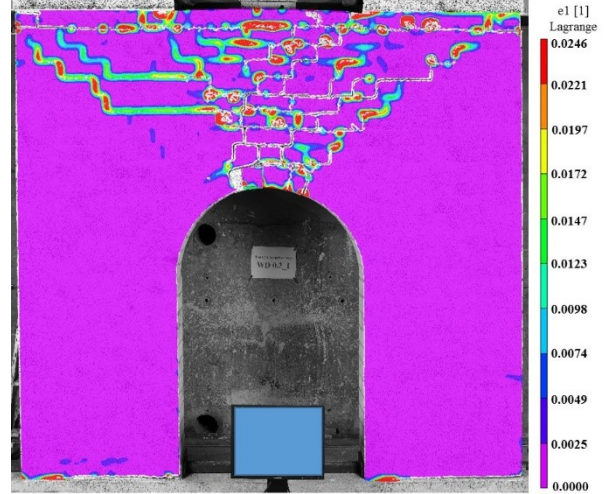


(h) WS_0.5_B (-36.0 mm)

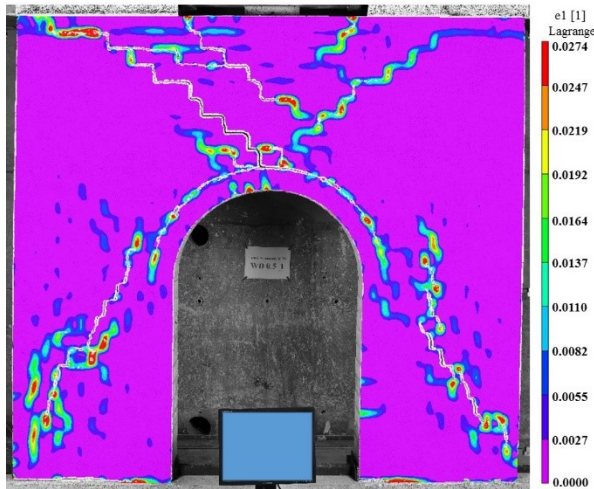
PERSON



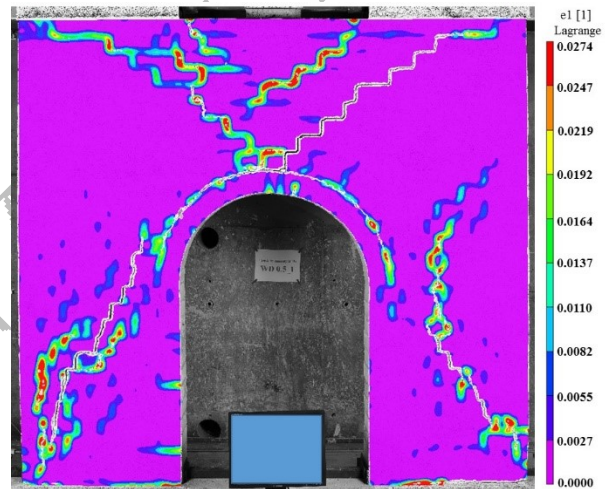
(i) WD_0.2 (+36.0 mm)



(j) WD_0.2 (-36.0 mm)

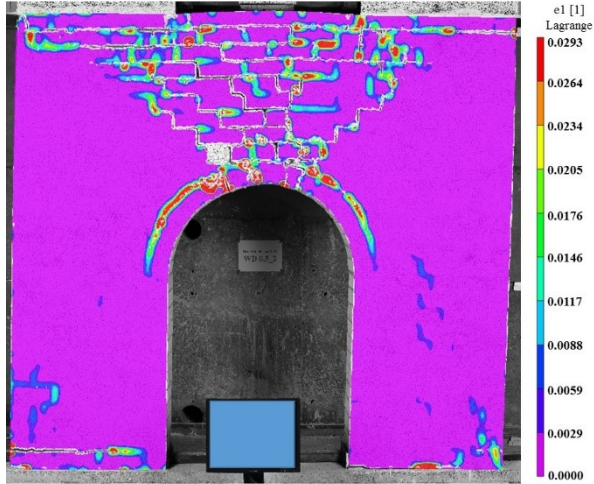


(k) WD_0.5_A (+24.0 mm)

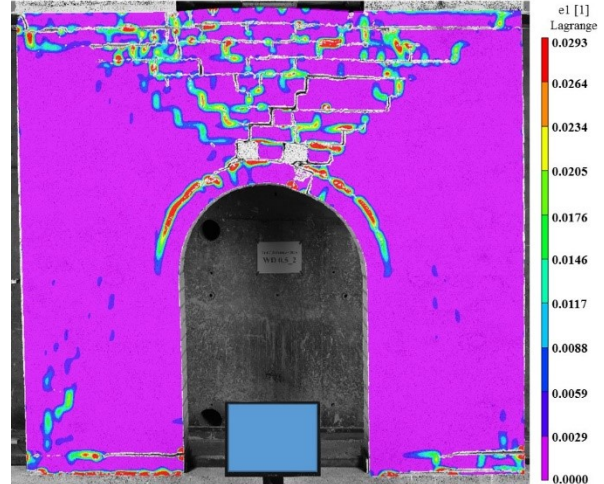


(l) WD_0.5_A (-24.0 mm)

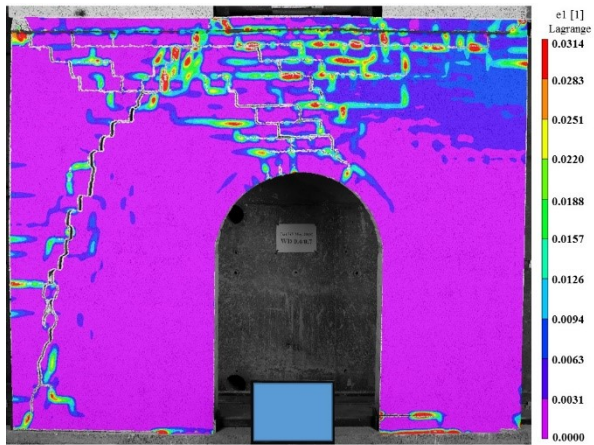
PERG



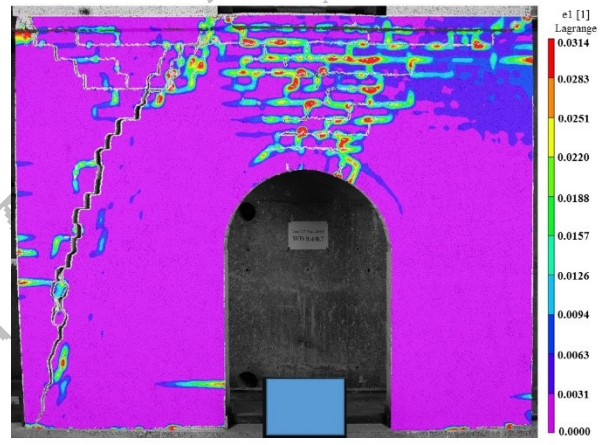
(m) WD_0.5_B (+48 mm)



(n) WD_0.5_B (-48 mm)

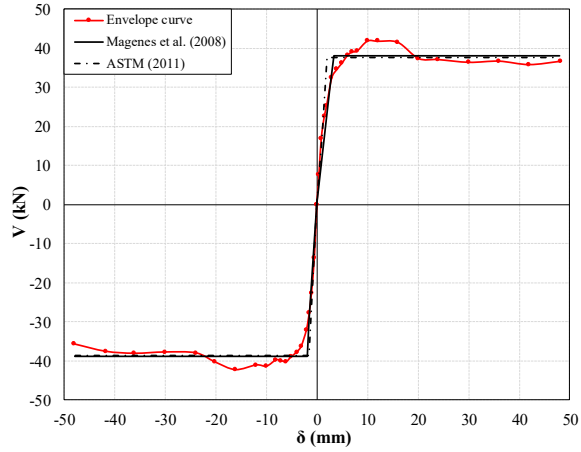


(o) WD_0.4/0.7 (+24.0 mm)

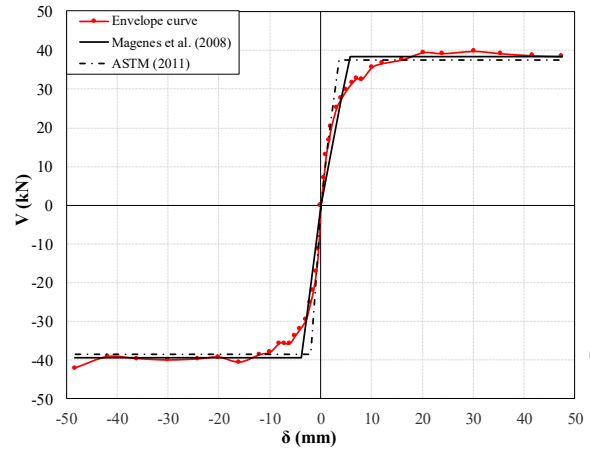


(p) WD_0.4/0.7 (-24.0 mm)

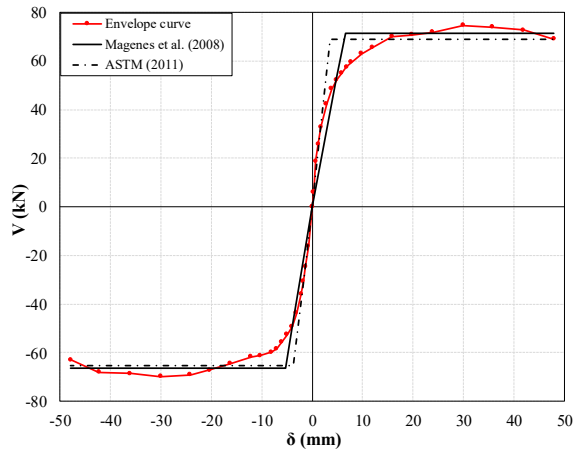
Fig. 8. Crack patterns of the URM walls at ultimate displacement



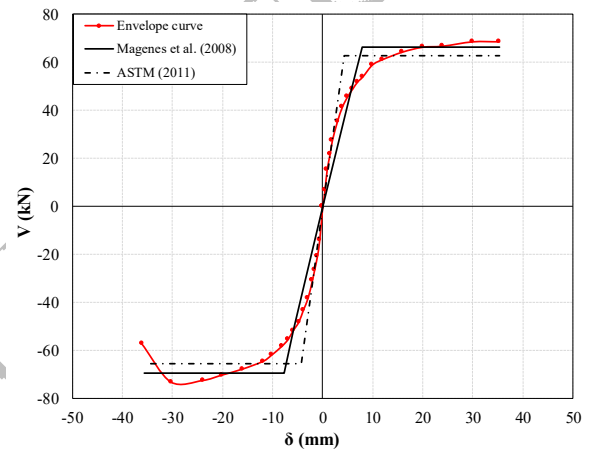
(a) WS_0.2_A



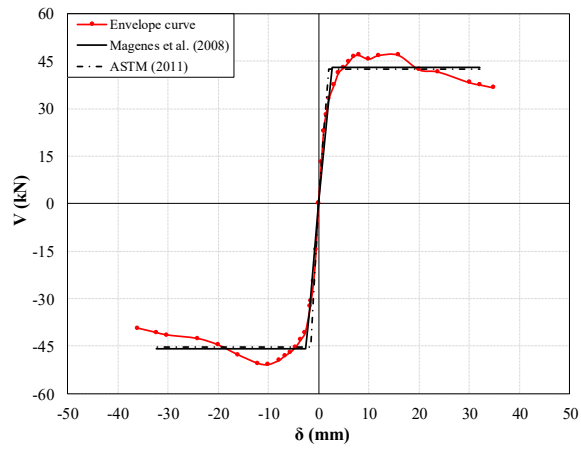
(b) WS_0.2_B



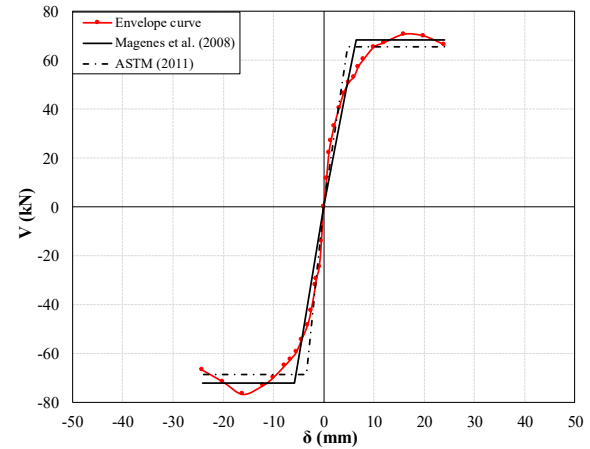
(c) WS_0.5_A



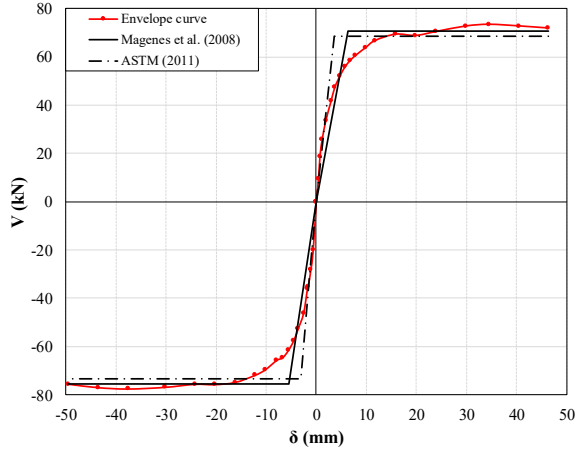
(d) WS_0.5_B



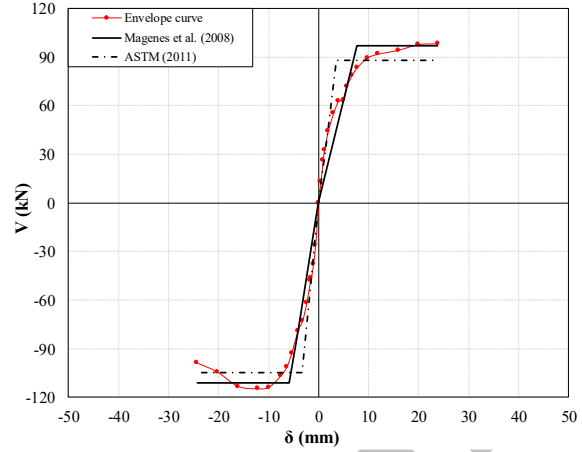
(e) WD_0.2



(f) WD_0.5_A



(g) WD_0.5_B



(h) WD_0.4/0.7

Fig. 9. Bilinearisation of the force-displacement behavior

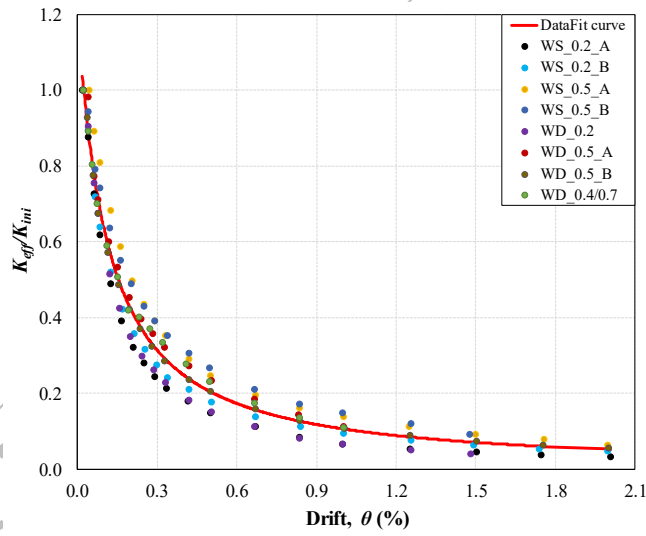
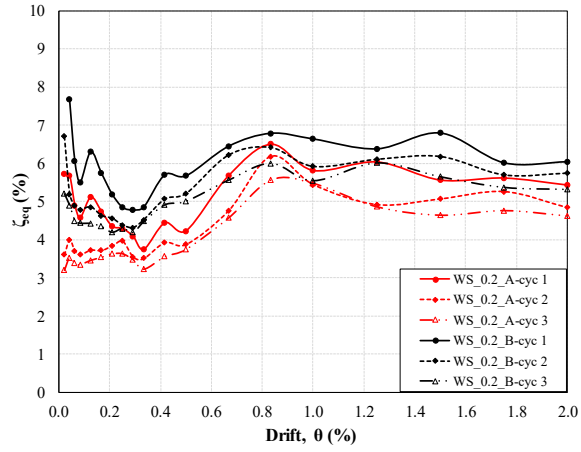
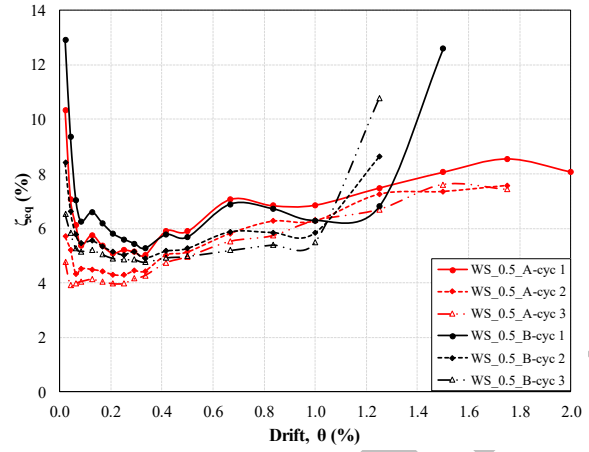


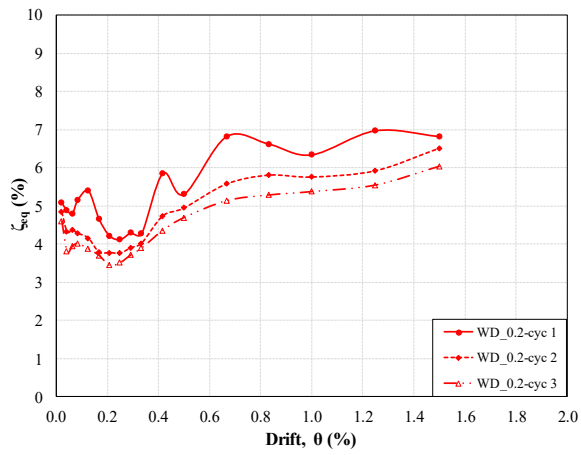
Fig. 10. Stiffness degradation pattern with the drift of the walls



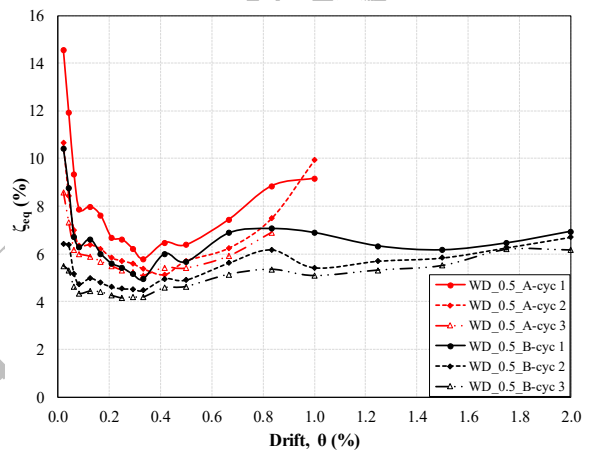
(a) WS_0.2



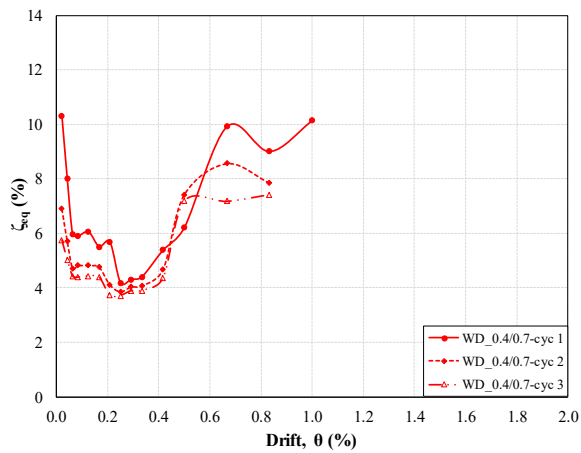
(b) WS_0.5



(c) WD_0.2



(d) WD_0.5



(e) WD_0.4/0.7

Fig. 11. Equivalent viscous damping of the tested walls

List of Tables

Table 1. Strengths of Different Mortar Types at Different Ages

Mortar Type	Flexural tensile strength of masonry (MPa) (COV %)			Compressive strength of mortar (MPa) (COV %)		
	Testing age			Testing age		
Lime: Sand= (1:3) Pozzolan added as % volume of lime	21 days	42 days	90 days	21 days	42 days	90 days
Rock lime without Pozzolan	--	--	0.056(25)	--	--	0.199(12)
Rock lime with 10% Pozzolan	--	--	0.069(26)	--	--	0.241(5)
Rock lime with 25% Pozzolan	0.052(29)	0.071(31)	0.077(28)	0.245(14)	0.307(4)	0.309(3)
Hydrated Lime	0.070(20)	0.071(10)	0.077(30)	0.212(4)	0.251(7)	0.543(0.1)
Cement: Lime: Sand = (1:2:9)	Testing age			Testing age		
	7 days	14 days	28 days	7 days	14 days	28 days
Rock lime-cement	0.212(38)	0.223(31)	0.201(50)	0.989(2)	1.229(9)	1.710(1)
Hydrated Lime-cement	0.621(29)	0.468(45)	0.402(44)	2.866(4)	4.120(5)	4.124(8)

Note: The lines below each of the bolded headings describe different mortar constituents which are mixed in the proportions shown in the bolded headings in each case.

Table 2. Mechanical Properties of the Materials

Name	Parameters	No. of tests	Mean Value	COV (%)	Unit
Brick unit	Brick compressive strength (f_b)	10	11.7	6	MPa
	Flexural tensile strength of brick (f_{ut})	10	1.1	23	MPa
Mortar joint	Mortar compressive strength (f_j)	9	1.7	2	MPa
	Direct tensile strength of mortar joint (f_{jt})	160		See Table 3	
	Joint cohesion (c)	9	0.15	a	MPa
	Joint coefficient of friction ($\tan\phi$)	9	0.74	a	--
Masonry prism	Masonry compressive strength (f_m)	6	7.0	7	MPa
	Elastic modulus (E_m)	6	2364	5	MPa

^aFor the shear test method in EN 1052-3 (CEN 2002), cohesion and coefficient of friction are determined from linear regression of the 9 data points and as such, COV values cannot be determined.

Table 3. Direct Tensile Strength of Mortar Joints Used to Construct the Walls

Wall Id	Batch No.	Curing time (days)	f_{mt} (MPa)	COV (%)	f_{jt} (MPa)
WS_0.2_A	1	151	0.077	28	0.052
	2		0.146	22	0.073
WS_0.2_B	1	30	0.115	58	0.077
	2		0.094	29	0.063
WS_0.5_A	1	31	0.169	11	0.113
	2		0.201	17	0.134
WS_0.5_B	1	29	0.178	27	0.119
	2		0.179	18	0.119
WD_0.2	1	46	0.181	39	0.121
	2		0.150	33	0.100
WD_0.5_A	1	40	0.075	17	0.050
	2		0.104	27	0.069
WD_0.5_B	1	31	0.193	23	0.129
	2		0.212	24	0.141
WD_0.4/0.7	1	50	0.225	37	0.150
	2		0.185	24	0.124
Average of all walls	--	--	0.155	26	0.102

Table 4. Result summary for the tested URM walls

Wall ID	V_{max} (kN)	δV_{max} (mm)	θV_{max} (%)	δ_u (mm)	θ_u (%)
WS_0.2_A (+)	41.9	10	0.42	48.28	2.01
WS_0.2_A (-)	-42.9	-16.11	-0.67	-48.05	-2.00
WS_0.2_B (+)	39.8	30.21	1.26	47.46	1.98
WS_0.2_B (-)	-42.1	-48.31	-2.01	-48.31	-2.01
WS_0.5_A (+)	74.6	29.92	1.25	47.96	2.00
WS_0.5_A (-)	-69.8	-30.05	-1.25	-47.92	-2.00
WS_0.5_B (+)	68.8	35.34	1.47	35.34	1.47
WS_0.5_B (-)	-73.1	-30.22	-1.26	-35.55	-1.48
WD_0.2 (+)	46.9	15.87	0.66	32.09	1.34
WD_0.2 (-)	-50.9	-10.05	-0.42	-32.33	-1.35
WD_0.5_A (+)	70.6	15.96	0.67	24.01	1.00
WD_0.5_A (-)	-76.7	-16.08	-0.67	-24.11	-1.00
WD_0.5_B (+)	73.4	34.57	1.44	46.38	1.93
WD_0.5_B (-)	-77.6	-37.59	-1.57	-49.59	-2.07
WD_0.4/0.7 (+)	98.3	23.84	0.99	23.84	0.99
WD_0.4/0.7 (-)	-114.9	-12.07	-0.50	-24.27	-1.01

Table 5. Bilinear parameters of the tested URM walls according to the method used in Magenes et al. (2008)

Wall ID	k_{el} (kN/mm)	V_u (kN)	V_u/V_{max} (--)	δ_e (mm)	μ (--)	Ω (--)	q (--)	$R=\Omega*q$ (--)
WS_0.2_A (+)	11.66	38.2	0.91	3.27	14.76	1.30	5.34	6.95
WS_0.2_A (-)	19.46	-38.9	0.92	-2.00	24.06	1.31	6.86	9.00
WS_0.2_B (+)	6.64	38.4	0.96	5.79	8.20	1.38	3.92	5.41
WS_0.2_B (-)	10.25	-39.4	0.94	-3.84	12.57	1.34	4.91	6.57
WS_0.5_A (+)	10.84	71.3	0.96	6.57	7.30	1.36	3.69	5.03
WS_0.5_A (-)	12.50	-66.2	0.95	-5.30	9.04	1.36	4.13	5.60
WS_0.5_B (+)	8.44	66.4	0.97	7.86	4.50	1.38	2.83	3.90
WS_0.5_B (-)	8.94	-69.3	0.95	-7.75	4.59	1.35	2.86	3.87
WD_0.2 (+)	16.08	43.1	0.92	2.68	11.97	1.31	4.79	6.30
WD_0.2 (-)	17.91	-45.9	0.90	-2.56	12.63	1.29	4.93	6.34
WD_0.5_A (+)	10.59	68.3	0.97	6.44	3.73	1.38	2.54	3.51
WD_0.5_A (-)	12.58	-72.4	0.94	-5.75	4.19	1.35	2.72	3.66
WD_0.5_B (+)	11.18	70.6	0.96	6.32	7.34	1.37	3.70	5.08
WD_0.5_B (-)	13.91	-75.4	0.97	-5.42	9.15	1.39	4.16	5.77
WD_0.4/0.7 (+)	12.69	97.2	0.99	7.66	3.11	1.41	2.29	3.23
WD_0.4/0.7 (-)	18.90	-111.0	0.97	-5.87	4.13	1.38	2.70	3.72

Table 6. Bilinear parameters of the tested URM walls according to the method used in ASTM (2011)

Wall ID	k_{el} (kN/mm)	V_u (kN)	V_u/V_{max} (--)	δ_e (mm)	μ (--)	Ω (--)	q (--)	$R=\Omega*q$ (--)
WS_0.2_A (+)	18.92	37.7	0.90	1.99	24.26	2.25	6.89	15.49
WS_0.2_A (-)	24.65	-38.7	0.91	-1.57	30.61	2.29	7.76	17.73
WS_0.2_B (+)	10.59	37.5	0.94	3.54	13.41	2.35	5.08	11.95
WS_0.2_B (-)	19.91	-38.6	0.92	-1.94	24.90	2.29	6.99	16.02
WS_0.5_A (+)	19.63	69.0	0.92	3.51	13.66	2.31	5.13	11.86
WS_0.5_A (-)	17.56	-65.2	0.93	-3.71	12.92	2.34	4.98	11.64
WS_0.5_B (+)	14.32	62.9	0.91	4.39	8.05	2.29	3.89	8.88
WS_0.5_B (-)	15.40	-65.7	0.90	-4.26	8.35	2.25	3.96	8.90
WD_0.2 (+)	22.16	42.6	0.91	1.92	16.71	2.27	5.69	12.94
WD_0.2 (-)	27.39	-45.2	0.89	-1.65	19.59	2.22	6.18	13.71
WD_0.5_A (+)	14.01	65.5	0.93	4.67	5.14	2.32	3.05	7.06
WD_0.5_A (-)	20.01	-68.6	0.89	-3.43	7.03	2.24	3.61	8.08
WD_0.5_B (+)	19.25	68.5	0.93	3.56	13.03	2.33	5.01	11.67
WD_0.5_B (-)	24.05	-73.5	0.95	-3.06	16.21	2.37	5.60	13.27
WD_0.4/0.7 (+)	24.52	88.2	0.90	3.60	6.62	2.24	3.50	7.85
WD_0.4/0.7 (-)	31.91	-104.7	0.91	-3.28	7.40	2.28	3.71	8.46

Table 7. Equivalent viscous damping with wall behaviour

Wall ID	Avg. ζ_{eq} (%)	COV (%)	Wall behaviour (deformation)		
			Left Pier	Right Pier	Spandrel
WS_0.2_A	4.48	19.3	Flexure	Flexure	Sliding
WS_0.2_B	5.36	14.3	Flexure	Flexure	Sliding
WS_0.5_A	5.61	23.4	Flexure	Flexure	Sliding
WS_0.5_B	5.92	25.4	Shear	Flexure	Sliding
WD_0.2	4.84	20.1	Flexure	Flexure	Sliding and Diagonal
WD_0.5_A	6.52	17.8	Shear	Shear	Diagonal
WD_0.5_B	5.43	15.9	Flexure	Flexure	Diagonal
WD_0.4/0.7	5.55	32.3	Shear	Flexure	Sliding and Diagonal

Table 8. Comparison of the measured with the predicted responses of URM walls

Wall Id	Lateral Strength (kN)			Stiffness (kN/mm)			Pier failure	
	Test	ASCE 41 (2013) (Error) %		Test	ASCE 41 (2013)	Test	ASCE 41 (2013)	
		Fixed-fixed	Fixed-free					Magenes et al. (2008)
WS_0.2	41.5	39.1 (-5.8)	21.7 (-47.7)	11.0	17.6	9.3	Rocking/toe crushing	Rocking
WS_0.5	71.6	88.1 (+23.0)	46.1 (-35.6)				Rocking/diagonal shear	Toe crushing
WD_0.2	48.9	49.5 (+1.2)	27.6 (-43.6)	13.7	21.1	17.9	Rocking	Rocking
WD_0.5	74.6	110.8 (+48.5)	58.2 (-21.9)				Rocking/diagonal shear	Toe crushing
WD_0.4/0.7	106.6	169.5 (+59.0)	89.3 (-16.2)	15.8	28.2	21.7	Rocking / diagonal shear	Toe crushing

Note: Lateral strengths for the wall tests represent the average of positive and negative loading directions and the average of two test specimens where repeat tests were conducted.